FRIGID ZONE **MEDICINE**
Original Article • DOI: 10. 1515/fzm-2024-0018

LCN2 aggravates diabetic cataracts by promoting ferroptosis in lens epithelial cells

Jiayue Zhang[1,2,3], Liyao Sun[1], Xiaohan Yu[1], Chen Yang[1], Qi An[1], Chaoqun Wei[1,2,3], Hongyan Ge[1*]

Abstract

Background: Cataracts are the leading cause of reversible blindness worldwide. Diabetic cataract (DC), a prevalent complication of diabetes mellitus, is characterized by its high occurrence, rapid progression, and severe impact. The prevalence of diabetes varies greatly between the northern and southern regions, with higher rates observed among northern residents. DC-induced lens opacity is mainly attributed to oxidative stress. However, it remains unclear whether ferroptosis, a form of regulated cell death, occurs in crystalline epithelial cells during the pathogenesis, which may represent a novel mechanism contributing to DC. **Methods:** Transmission electron microscopy, quantitative assays for iron levels and reactive oxygen species (ROS), real-time quantitative polymerase chain reaction (RT-qPCR), western blotting, immunofluorescence, and immunohistochemistry were used to detect ferroptosis. Gene editing techniques were utilized to study the regulatory relationships among lipocalin 2 (LCN2), glutathione peroxidase 4 (GPX4), and ferritin heavy chain (FTH). Local knockdown of the LCN2 gene in B-3 cells and the eyes of Sprague Dawley (SD) rats was performed to verify and further explore the role and regulatory mechanisms of LCN2 in DC-associated ferroptosis. **Results:** An *in vitro* model using high glucose levels and an *in vivo* model with streptozotocin-induced diabetes in SD rats were successfully established. Ferroptosis was observed in both *in vitro* and *in vivo* experiments. LCN2 protein was normally expressed in human and rat lens epithelial cells, but its expression significantly increased during ferroptosis. The ferroptosis inhibitor, ferrostatin-1 (Fer-1) effectively inhibited ferroptosis and reduced LCN2 protein expression. Notably, local knockdown of LCN2 *via* gene editing protected lens epithelial cells from ferroptosis *in vitro* and slowed the progression of DC in SD rats *in vivo*. **Conclusion:** Our findings underscore the significant role of ferroptosis in the pathogenesis of DC, suggesting that selectively targeting LCN2 activation and enhancing ferroptosis resistance may offer a novel therapeutic approach for treating DC.

Keywords

lipocalin-2; ferroptosis; diabetic cataracts

Received 05 August 2024, accepted 09 August 2024

[1]*Eye Hospital, First Affiliated Hospital, Harbin Medical University, Harbin 150001, China*
[2]*Key Laboratory of Ischemia-reperfusion, Harbin Medical University, Ministry of Education, Harbin 150001, China*
[3]*Experimental Animal Centre, the Second Affiliated Hospital, Harbin Medical University, Harbin 150001, China*

**Corresponding author Hongyan Ge, E-mail: gehongyan@hrbmu. edu. cn*

1 Introduction

In recent years, the rising incidence of diabetes mellitus (DM) has led to an increase in the prevalence of diabetic cataracts (DC), the most common ocular complication of diabetes[1-4]. Diabetic individuals are approximately five times more likely to develop cataracts than those without the condition. Typically, DC emerges gradually within a few years after the diagnosis of diabetes and progresses rapidly[5-9]. Although surgical intervention is the standard treatment for DC, it carries risks of complications and imposes significant financial burdens[10]. Therefore, understanding the pathogenesis of DC and developing early treatment strategies to delay its progression are of paramount importance. However, the mechanisms underlying DC and related therapeutic targets remain inadequately understood.

Ferroptosis, a newly recognized form of cell death driven by oxidative stress and regulated by various cellular metabolic pathways, including glucose metabolism, has been implicated in numerous signaling pathways associated with various diseases[11]. Initially observed in cancer cells[12], recent studies indicate its involvement in the damage to multiple organs and degenera-

tive conditions, such as myocardial ischemia-reperfusion injury, cardiomyopathy, and diabetes-induced nephropathy[13-15]. As a result, research on ferroptosis has gradually expanded beyond cancer to encompass benign diseases, showing great potential for treating oxidative stress-related conditions. However, whether ferroptosis occurs in lens epithelial cells during the pathogenesis of DC-potentially representing a novel mechanism contributing to DC-remains unclear.

LCN2, a neutrophil gelatinase-related lipid carrier protein, is a multifunctional glycoprotein encoded by a gene located on chromosome 9q34.11[16]. LCN2 is involved in various physiological processes, including cell differentiation, migration, and apoptosis, and can contribute to inflammatory responses by increasing the levels of inflammatory factors[17-19]. Furthermore, as an inflammatory factor, LCN2 has been linked to the development of insulin resistance and obesity, suggesting its potential as a therapeutic target for obesity-related metabolic and cardiovascular diseases[20]. Despite extensive studies into its diagnostic and therapeutic value, the expression of LCN2 in lens epithelial cells and its role in regulating cell death mechanisms in DC remain unclear.

To investigate the role of LCN2 in DC and its relationship with ferroptosis, we conducted preliminary *in vitro* experiments using a high glucose-concentration model and *in vivo* experiments with intraperitoneal streptozotocin (STZ) injection in a Sprague Dawley (SD) rat DC model. Our study aimed to examine the involvement of ferroptosis in DC development, determine whether LCN2 is expressed in human and rat lens epithelial cells, assess how differential expression of LCN2 affects the severity of ferroptosis, and explore the possible mechanisms by which LCN2 contributes to the pathogenesis of DC.

2 Materials and Methods

2.1 Materials

The human lens epithelial cell line B-3 (B-3) was purchased from American Type Culture Collection (ATCC Cat# CRL-11421, RRID: CVCL_6367). Fetal bovine serum (FBS) was procured from Gibco (Thermo Fisher Scientific, Inc. , Waltham, MA, USA), and Dulbecco's modified Eagle medium (DMEM) was purchased from VivaCell Shanghai (Shanghai, China). The Cell Counting Kit-8 (CCK-8) was sourced from Merck (Darmstadt, Germany). The Iron Assay Kit was obtained from BioVision (San Francisco, CA, USA), and the ROS Assay Kit from Beyotime Biotechnology (Shanghai, China). Easyscript® reverse transcriptase and TransStart® Green qPCR SuperMix was purchased from Transgen Biotech (Beijing, China). TRIzol reagent and primers were purchased from Invitrogen (Eugene, OR, USA). Primary and fluorescent-labeled secondary antibodies were obtained from Proteintech (Chicago, IL, USA). STZ was purchased from Sigma-Aldrich (St. Louis, MO, USA), and small molecule inhibitors were acquired from MedChemExpress (Monmouth Junction, NJ, USA).

2.2 Cell culture and transfection

Cells were cultured in DMEM supplemented with 15% FBS at 37°C in a 5% CO_2 atmosphere. When the cells reached the logarithmic growth phase and 70% confluence, they were prepared for the relevant experiments. A small interfering RNA (siRNA) targeting LCN2 was designed and synthesized by Ruibo Biotechnology limited company (Guangzhou, China). The siRNA sequence with the highest knockdown efficiency among the three designed sequences was selected for use. B-3 cells were transfected with siRNA (100 pmol/L) using Lipofectamine™ 2000.

2.3 Animals

Six-week-old male SD rats were purchased from the Experimental Animal Center of the Second Affiliated Hospital of Harbin Medical University. The study was approved by the Institutional Review Board (or Ethics Committee) of the First Affiliated Hospital of Harbin Medical University (IACUC: 2022020 and date of approval: April 8, 2022).

2.4 Establishment of the high glucose-induction model

2.4.1 High glucose-induced cell model

B-3 cells were cultured under optimal conditions and seeded into six-well cell culture plates. Once the cells were attached, they were rinsed twice with pre-warmed, cell-specific phosphate-buffered saline (PBS). Then, 2.5 mL of pre-prepared cell culture medium containing varying concentrations of glucose (5.5, 10, 20, 40, 60, 80, and 100 mmol/L) was added to each well. The plates were then incubated in a constant temperature incubator for 48 h.

2.4.2 Animal model of DC in SD rats induced by intraperitoneal injection of STZ

Specific pathogen-free-grade SD rats, weighing 200 ± 20 g, were used in this study. The housing conditions were maintained at a temperature of 22 ± 1°C and humidity levels between 45% and 55%. Prior to the experiments, the rats underwent a 7-day adaptation period during which systemic and ocular diseases were excluded. To evaluate the effects of glucose-induced cataracts and ferrostatin-1 (Fer-1) on the progression of cataracts, three animal model groups were established. The first group served as a blank control, while the second group was the DC model group, which received intraperitoneal injections of STZ at a dose of 65 mg/kg.

In the third group, 65 mg/kg STZ was prepared and used immediately, with injections completed within 10 min.

Fasting blood glucose levels (FBG) were measured in all rats before the injections and at 1, 3, 5, and 7 days post-injection. FBG levels of > 16.7 mmol/L were used to confirm the induction of DM. Weight and FBG levels were measured and recorded weekly. Starting on the day of the intraperitoneal injection, all rats were anesthetized every other day with a mixture of 90 mg/kg ketamine and 15 mg/kg xylazine. Their eyes were dilated with tropicamide eye drops, and after pupil enlargement, the degree of lens opacity was observed and recorded under a microscope.

Subsequently, 500 mmol/L Fer-1 and an equivalent dose of dimethyl sulfoxide (DMSO) for dissolving the drug were injected into the rat subconjunctiva (5 μL/eye) using a 28-gauge microneedle and a Hamilton microsyringe at daily intervals until the end of the experiment. At the 12th week, the rats were euthanized *via* CO_2 asphyxiation, and their eyeballs were removed and placed in isotonic saline containing 1% penicillin and streptomycin. The intact lenses were hen carefully removed using ophthalmic microsurgical instruments under an ophthalmic dissecting microscope. Each rat lens was labeled with its group and serial number in the microscopic imaging system. They were photographed and recorded under uniform lighting and at the same distance. Portions of the lenses were fixed in 4% paraformaldehyde for subsequent frozen sectioning and immunohistochemical staining experiments. The remaining lenses were processed using the central continuous ring capsule method to peel off the anterior capsule membrane, followed by storage at -80°C for subsequent experiments.

2.5 Knockdown of LCN2 locally *in vivo*

To demonstrate that decreased LCN2 expression decreases lens opacity *in vivo*, SD rats were randomly divided into four groups: control siRNA, LCN2 siRNA, DC, and LCN2 siRNA + DC. All rats underwent siRNA transfection into the eye using Polyplus in vivo-jetPEI® as the transfection medium. In each rat, one eye was transfected with LCN2 siRNA to knockdown the LCN2 gene in the anterior segment, while the other eye was transfected with control siRNA. Specifically, 25 μg of LCN2 siRNA or control siRNA was evenly mixed with 50 μL of transfection working solution containing 3 μL of in vivo-jetPEI®. The transfection complex was then rapidly administered *via* subconjunctival injection, with 5 μL injected into each eye.

2.6 CCK-8

Cells were seeded in 96-well plates at a density of 1 × 104 cells per well and treated with various glucose concentrations (5.5, 10, 20, 40, 60, 80, and 100 mmol/L). The plates were then incubated for 48 h at 37°C i. Following this, 10 μL of CCK-8 solution was added to each well, and the cells were incubated for an additional hour. The optical density (OD) at 450 nm was measured using a microplate reader.

2.7 RT-PCR

The expression levels of ferritin heavy chain (FTH1), glutathione peroxidase 4 (GPX4), solute carrier family 7 member 11 (SLC7A11), and LCN2 mRNA were determined by RT-PCR using EasyScript® reverse transcriptase. All primer sequences are listed in Table 1. Total RNA was extracted from cells and reverse transcribed into cDNA according to the manufacturer's instruction. RT-PCR amplification was performed using a 10-μL reaction system containing 700 ng cDNA, 3.6 μL water, 5 μL of TransStart® Green qPCR SuperMix, 0.2 pmol/L reverse primer, and 0.2 pmol/L forward primer. The RT-PCR was performed on a real-time PCR system (Bio-Rad, Hercules, CA, USA). The mRNA expression levels were normalized to the housekeeping gene using the 2-ΔΔCt method.

2.8 Total cellular protein extraction

Cells or tissues were first rinsed once with PBS. Subsequently, they were lysed using radioimmunoprecipitation assay (RIPA) buffer (Boston BioProducts, Boston, MA, USA) supplemented with 1 mmol/L phenylmethylsulfonyl fluoride (PMSF). The lysates were collected in a centrifuge tube and incubated on ice for lysis. After gentle mixing, the lysate was centrifuged at 12, 000 rpm for 20 min at 4°C. The supernatant was then transferred to a new centrifuge tube and combined with an equal volume of protein loading buffer. The mixture was heated in a 100°C metal bath for 7 min, cooled to 25°C, and subsequently stored at -20°C until further experimental analysis.

2.9 Western blotting (WB) analysis

Protein concentrations were quantified using the Pierce™ BCA Protein Quantification Kit (Thermo Fisher Scientific, Inc.), and the appropriate volume of each sample was determined. Proteins

Table 1 All primer sequences

Primer	Nucleotide sequence (5′ - 3′)
GPX4	F-CGATACGCTGAGTGTGGTTT- R-CGGCGAACTCTTTGATCTCTT-
FTH1	F-TACCTGAATGAGCAGGTGAAAG- R-GATATTCCGCCAAGCCAGAT-
SLC7A11	F-GGTTGCCCTTTCCCTCTATTC- R-CCTGGGTTTCTTGTCCCATATAA-
LCN2	F-CCAGGACAACCAATTCCAGGG- R-GTGGCATACATCTTTTGCGGG-
GAPDH	F-CTGGGCTACACTGAGCACC- R-AAGTGGTCGTTGAGGGCAATG-

F, forward primer; R, reverse primer

were separated using 12.5% sodium dodecyl sulfate-polyacrylamide gel electrophoresis (SDS-PAGE), then transferred onto a polyvinylidene fluoride (PVDF) membrane (Millipore). The PVDF membrane (Millipore) was blocked with 5% skim milk in Tris-buffered saline with 0.05% Tween 20 (TBST) for 1 hour at room temperature. The membrane was then incubated overnight at 4°C with primary antibodies diluted in TBST. The primary antibodies used were: mouse anti-GPX4 (Proteintech Cat# 67763-1-Ig, RRID: AB_2909469) at 1：3000, rabbit anti-FTH1 (Proteintech Cat# 10727-1-AP, RRID: AB_2278673) at 1：6000, rabbit anti-SLC7A11 (Proteintech Cat# 26864-1-AP, RRID: AB_2880661) at 1：1500, rabbit anti-LCN2 (Proteintech Cat# 26991-1-AP, RRID: AB_2880715) at 1：1000, and rabbit anti-GAPDH (Proteintech Cat# 10494-1-AP, RRID: AB_2263076) at 1：20,000.

The following day, the membrane was incubated with the appropriate HRP-conjugated secondary antibodies: Affinipure Goat Anti-rabbit IgG (H+L) (Proteintech Cat# SA00001-2, RRID: AB_2722564) at 1：10000 or Affinipure Goat Anti-mouse IgG (H+L) (Proteintech Cat# SA00001-1, RRID: AB_2722565) at 1：8000, for 1h at 25°C. Protein bands were visualized using an enhanced chemiluminescence (ECL) assay kit and images were captured.

2.10 Immunofluorescence (IF) staining

Cells were seeded in 24-well plates at a density of 2.5 × 10^5 cells/well. After glucose incubation or treatment, cells were rinsed twice with pre-cooled PBS, fixed in 4% paraformaldehyde, and permeabilized with 0.5% Triton X-100 for 20 min. Blocking was performed with 5% goat serum at 25°C for 1 h. Primary antibodies diluted in 5% goat serum was then added and incubated overnight at 4°C. The primary antibodies used were: mouse anti-GPX4 (Proteintech Cat# 67763-1-Ig, RRID: AB_2909469) at 1：500, rabbit anti-FTH1 (Proteintech Cat# 10727-1-AP, RRID: AB_2278673) at 1：50, and rabbit anti-LCN2 (Proteintech Cat# 26991-1-AP, RRID: AB_2880715) at 1：300.

The following day, cells were incubated with fluorescent secondary antibodies: H&L (CoraLite® 488) donkey anti-rabbit IgG (Proteintech Cat# SA00013-6, RRID: AB_2890972) at 1：300 and H&L (CoraLite® 594) donkey anti-mouse IgG (Proteintech Cat# SA00013-7, RRID: AB_2890973) at 1：300, both diluted in 5% goat serum, for 1 h at 25°C. Nuclei were stained with DAPI for 5 min, followed by anti-fluorescent quenching tablets to prevent signal fading. Cells were examined under a Zeiss Observer A1 fluorescence microscope and images were captured using the ZEN microscope camera system.

2.11 Immunohistochemistry (IHC) staining

Fresh, intact lenses from SD rats lenses were rinsed with PBS, rapidly frozen in liquid nitrogen, and sectioned using a microtome. The sections were mounted on slides and allowed to air- dry. They were then fixed with 4% pre-cooled paraformaldehyde for approximately 15 min, and then permeabilized with 0.3% Triton-100 for 15 min. Antigen retrieval was performed in EDTA buffer, followed by blocking with goat serum for 1 h at 25°C; subsequently, primary antibody diluted in goat serum was added, followed by incubation at 4°C overnight.

The primary antibodies, diluted in goat serum, were applied and incubated overnight at 4°C. The primary antibodies used were: mouse anti-GPX4 (Proteintech Cat# 67763-1-Ig, RRID: AB_2909469) at 1：2000 and rabbit anti-FTH1 (Proteintech Cat# 10727-1-AP, RRID: AB_2278673) at 1：300.

On the following day, after removing the primary antibodies, a secondary antibody enhancer was applied at 25°C. Detection was carried out using a two-step mouse/rabbit detection kit (ZSGB-BIO, Beijing, China) with secondary antibodies diluted in goat serum, and incubated for 30 min at 25°C. Sections were then subjected to DAB staining for 30 s, rinsed with water for 10 min, and counterstaining with hematoxylin for 3 min. Following a final rinse in water, sections were dehydration through 95% and 100% ethanol, cleared with xylene, and mounted with neutral gum.

Stained sections were examined under a Zeiss biological optical microscope and images were captured using the ZEN microscope software version 2.0 (ZEN Digital Imaging for Light Microscopy, RRID: SCR_013672).

2.12 Iron assay

Following the manufacturer's instructions, an appropriate amount of the iron-reducing agent was added to the sample and allowed to stand at 25°C in the dark for 30 min to reduce Fe^{3+} to Fe^{2+}. The reaction was terminated by adding an iron-ion probe. The OD at 593 nm was measured using a microplate reader, and the concentration of iron ions in the resulting sample was determined as the Fe^{2+}/Fe^{3+} ratio.

2.13 Reactive oxygen species (ROS) assay

Cells were washed with PBS, collected in centrifuge tubes, counted, and recorded. A 1 mL solution of DCFH-DA, prepared according to the instructions, was added, and the cells were resuspended. The cells were then incubated at 37°C in light for 30 min, with the centrifuge tubes mixed every 5 min. Then, the cells were centrifuged at 1000 ×g for 5 min, and the pellet was resuspended in PBS. Finally, the cells were transferred back to the original 96-well plate, and the OD was measured using a microplate reader according to the manufacturer's instructions.

2.14 Transmission electron microscopy

The cells were rinsed with PBS, collected in centrifuge tubes, centrifuged at 1000 ×g for 5 min. The supernatant was discarded, and the cell pellet was fixed in 2.5% glutaraldehyde solution (pH 7.2) in a 0.1 mol/L buffer and incubated at 4°C overnight. The following day, the samples were refixed with 1% osmium tetroxide solution and incubated at 4°C for approximately 2 h. Next, the cells were dehydrated through a graded series of ethanol (50%, 70%, 90%, and 100%) and then through 100% acetone. Each dehydration step was performed by centrifugation for 9 min. The samples were then saturated with pure acetone and an embedding solution. After embedding and polymerization, the samples were sectioned using an ultrathin microtome to a thickness of 50-60 nm. The sections were double stained with uranyl acetate and lead citrate. The cell ultrastructure, with particular attention to mitochondrial structures, was examined and documented using transmission electron microscopy.

2.15 Statistical analysis

Statistical analysis was performed using SPSS 26.0 (RRID: SCR_002865), and GraphPad Prism 7 (RRID: SCR_002798) software was used for data visualization. Measurement data are expressed as mean ± standard deviation. Comparisons between two groups were made using the independent sample *t*-test. For multi-group comparisons, one-way analysis of variance (ANOVA) was employed, with pair-wise comparisons performed using the least significant difference (LSD) method. The Welch test was used for comparisons involving unequal variances, and the Dunnett *t*-test was used for comparisons against a control group. Body weight and blood glucose data in rats were analyzed using a two-factor repeated-measures ANOVA. Statistical significance was defined as $P < 0.05$.

3 Results

3.1 Glucose dose-dependent induction of ferroptosis in B-3 cells

Initially, different concentrations of glucose medium were prepared to induce B-3 cells. The CCK-8 assay was employed to determine the optimal glucose concentration for the *in vitro* model for further experiments. Results showed that B-3 cell survival significantly decreased with glucose concentrations of 5.5, 10, 20, 40, 60, 80, and 100 mmol/L, with survival dropping to around 50% at 40 mmol/L glucose (Fig. 1A). Consequently, 40 mmol/L glucose was chosen for further experiments. To control for osmolarity factors, cells were divided into five groups: a blank control with 5.5 mmol/L glucose, a hypertonic control with 5.5 mmol/L glucose plus 40 mmol/L mannitol, and high glucose induction groups with 10, 20, and 40 mmol/L glucose. Transcriptional and protein level analyses compared these to the blank control. The expression levels of FTH1, GPX4, and SLC7A11 did not differ significantly in the mannitol hypertonic controls, but were reduced in a dose-dependent manner in glucose-induced B-3 cells (Fig. 1B-D). At 40 mmol/L glucose, protein expression decreased by about 50%. Iron (Fe^{2+}/Fe^{3+}) and ROS levels also increased with glucose concentration (Fig. 1E, F). Osmotic pressure effects were ruled out, and the hypertonic control group was omitted in subsequent experiments. Cells from the remaining four groups were analyzed using transmission electron microscopy, revealing glucose-induced mitochondrial shrinkage, increased membrane density, color deepening, reduced or absent cristae, and outer membrane rupture, with these changes becoming more pronounced at higher glucose concentrations. Nuclear changes were minimal across all groups (Fig. 1G). Immunofluorescence experiments further confirmed a ferroptosis-like phenotype in glucose-induced B-3 cells, with decreased fluorescence intensity of FTH1 and GPX4 proteins at higher glucose concentrations, particularly significant in the 40 mmol/L glucose group (Fig. 1H-K).

3.2 High glucose increases the expression of LCN2 in B-3 cells

To investigate the effect of LCN2 expression in B-3 cells and the effect of glucose induction on LCN2 expression levels, we established three experimental groups: a negative control, a group with media containing 40 mmol/L mannitol, and a group with 40 mmol/L glucose. At both the transcriptional and protein levels, results revealed no significant difference in LCN2 expression between the mannitol-treated group and the negative control. However, LCN2 was significantly increased in glucose-induced B-3 cells, increasing more than threefold compared to controls (Fig. 2A-C). Immunofluorescence experiments corroborated these findings, showing a marked increase in LCN2 fluorescence intensity in the 40 mmol/L glucose induction group compared to the control group (Fig. 2D, E).

3.3 Fer-1 inhibits high glucose-induced ferroptosis in B-3 cells

To investigate whether high glucose concentrations induce ferroptosis, we divided the cells into three groups: a DMSO control, a 40 mmol/L glucose group, and a group pretreated with the ferroptosis inhibitor Fer-1 plus 40 mmol/L glucose. We assessed LCN2, GPX4, FTH1, and SLC7A11 at the transcriptional and protein levels. Results showed that LCN2, GPX4, FTH1, and SLC7A11 expression were significantly lower in the Fer-1 pretreated cells compared to those treated with 40 mmol/L glucose alone (Fig. 3C-E), indicating that Fer-1 pretreatment reduced ferroptosis in B-3 cells and potentially lowered LCN2 expression levels. Corresponding measurements of iron (Fe^{2+}/Fe^{3+}) and ROS

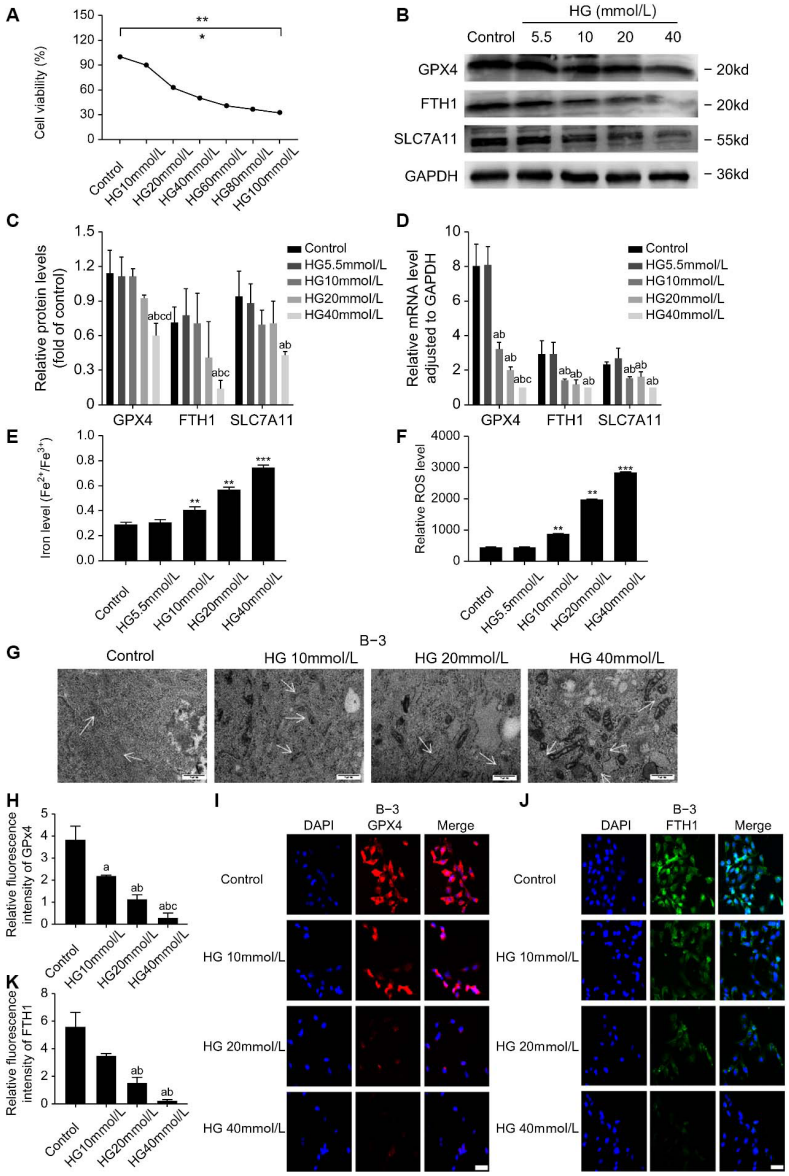

Fig. 1 High glucose induces ferroptosis in B-3 cells in a dose-dependent manner

(A) To analyze the effect of high glucose concentrations on B-3 cell viability, CCK-8 assays were performed after treating the cells with culture media containing glucose at concentrations of 5.5, 10, 20, 40, 60, 80, and 100 mmol/L. The results are presented from three independent experiments. (B-D) The results of RT-PCR and Western blot analysis of GPX4, FTH1 and SLC7A11 when B-3 cells were treated with glucose concentration of 5.5 mmol/L and glucose concentration of 5.5 mmol/L + mannitol concentration of 40 mmol/L. Results of RT-PCR and Western blot analysis of GPX4, FTH1, and SLC7A11 when B-3 cells were treated with glucose at concentrations of 10, 20, or 40 mmol/L. The results are presented from three independent experiments. (a: Compared with the control group, b: compared with the 40 mmol/L mannitol group, c: compared with the 10 mmol/L high glucose group, d: compared with the 20 mmol/L high glucose group, all $P < 0.05$) (E-F) Iron levels (Fe^{2+}/Fe^{3+}) and ROS levels in B-3 cells treated with glucose at concentrations of 5.5, 10, 20, or 40 mmol/L and glucose at a concentration of 5.5 mmol/L plus mannitol at a concentration of 40 mmol/L. The results are presented from three independent experiments. ($^{**}P < 0.01$; $^{***}P < 0.005$) (G) When B-3 cells were treated with glucose at concentrations of 5.5, 10, 20, or 40 mmol/L, the ultrastructure of the cells was photographed by TEM. (H-K) When B-3 cells were treated with 5.5 mmol/L glucose and 5.5 mmol/L glucose + 40 mmol/L mannitol, the relative fluorescence intensity of GPX4 and FTH1 was measured by IF staining. When B-3 cells were treated with glucose at concentrations of 10, 20, or 40 mmol/L, the relative fluorescence intensities of GPX4 and FTH1 were measured by the IF staining method. The results are presented from three independent experiments. (a: Compared with the control group, b: compared with the 10 mmol/L high glucose group c: compared with the 20 mmol/L high glucose group, all $P < 0.05$).

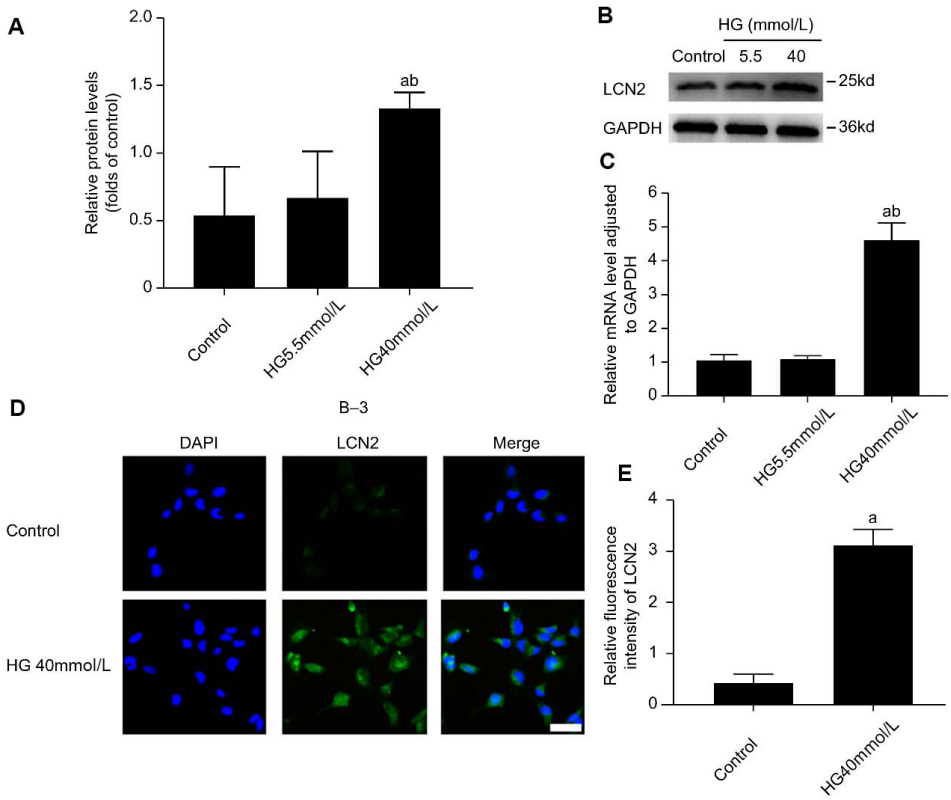

Fig. 2 High glucose-induced differential expression of LCN2 in B-3 cells

(A-C) A blank control group and a high osmotic pressure control group were set up, and that result of RT-PCR and Western blot analysis of LCN2 are obtained when B-3 cells are treated with glucose concentration of 5.5 mmol/L, glucose concentration of 5.5 mmol/L + mannitol concentration of 40 mmol/L and glucose concentration of 40 mmol/L. The results are presented from three independent experiments. (D-E) A blank control group and a high osmotic pressure control group were set up. When B-3 cells were treated with glucose concentration of 5.5 mmol/L, glucose concentration of 5.5 mmol/L + mannitol concentration of 40 mmol/L and glucose concentration of 40 mmol/L, the relative fluorescence intensity of LCN2 was measured by if staining method. The results are presented from three independent experiments. (a: Compared with the control group, b: compared with the 40 mmol/L mannitol group, all $P < 0.05$).

levels confirmed significant reductions in the Fer-1 pretreated cells compared to the glucose-treated group (Fig. 3A, B). Immunofluorescence analysis further demonstrated that LCN2 fluorescence intensity was markedly reduced in the Fer-1 pretreatment group, while GPX4 and FTH1 intensities were significantly higher (Fig. 3F-K). Ultrastructural examination by transmission electron microscopy revealed that, compared to the Fer-1 pretreatment group, B-3 cells in the 40 mmol/L glucose group had larger volumes, lower membrane density, lighter color, fewer mitochondrial cristae, and less outer membrane rupture (Fig. 3l). These findings suggest that Fer-1 pretreatment significantly mitigates glucose-induced ferroptosis in B-3 cells, likely due to the reduction in LCN2 expression.

3.4 LCN2 silencing inhibits high glucose-induced ferroptosis in B-3 cells

To investigate how differential expression of the LCN2 protein affects glucose-induced ferroptosis in B-3 cells, we performed LCN2 gene knockdown using siRNA. The experimental groups were divided into four: siRNA control, LCN2 siRNA, 40 mmol/L high glucose, and LCN2 siRNA + 40 mmol/L high glucose. Protein level analysis confirmed efficient knockdown of LCN2, with no significant differences in LCN2, GPX4, and FTH1 expression between the siRNA control and LCN2 siRNA groups. However, a significant decrease in GPX4 and FTH1 levels was observed in the 40 mmol/L high glucose group. In contrast, in the LCN2 siRNA + 40 mmol/L glucose group, GPX4 and FTH1 expression levels increased significantly compared to the 40 mmol/L high glucose group (Fig. 4A, B). These results suggest that knocking down LCN2 effectively mitigates high glucose-induced ferroptosis in B-3 cells.

3.5 Development of cataracts in diabetic SD rats

Based on our *in vitro* results, we developed a diabetes model us-

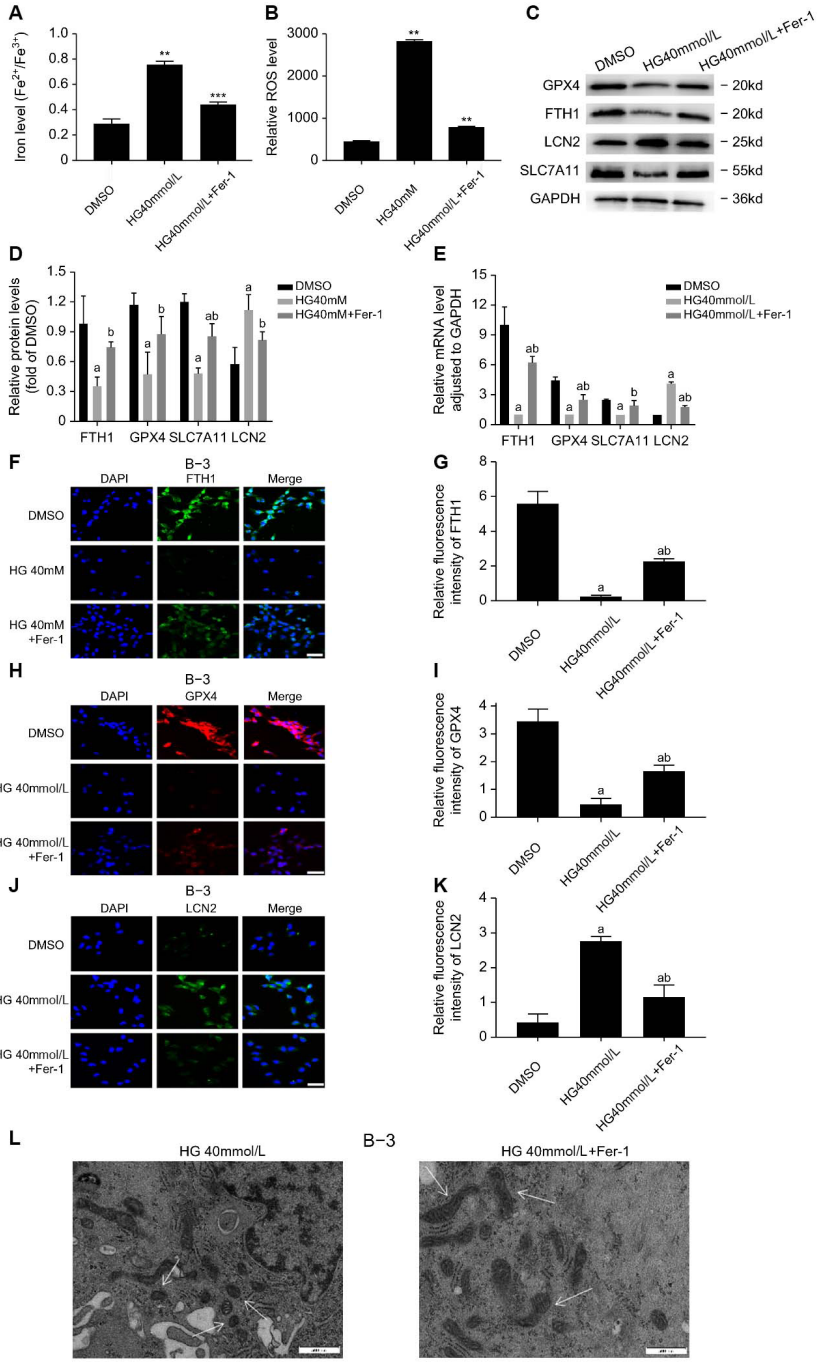

Fig. 3 Fer-1 rescues high glucose-induced ferroptosis in B-3 cells

(A-B) Iron levels (Fe^{2+}/Fe^{3+}) and ROS levels in B-3 cells treated with DMSO, high glucose at a concentration of 40 mmol/L or Fer-1. The results are presented from three independent experiments. (C-E) Results of RT-PCR and Western blot analysis of GPX4, FTH1, LCN2 and SLC7A11 in B-3 cells treated with DMSO, high glucose at a concentration of 40 mmol/L, Fer-1. The results are presented from three independent experiments. (a: Compared with the DMSO group, b: compared with the 40 mmol/L high glucose group, all $P < 0.05$) (F-K) When B-3 cells were treated with DMSO, 40 mmol/L high glucose or Fer-1, the relative fluorescence intensity of GPX4, FTH1, and LCN2 was measured by IF staining method. The results are presented from three independent experiments. (a: Compared with the DMSO group, b: compared with the 40 mmol/L high glucose group, all $P < 0.05$). (L) When B-3 cells were treated with glucose at concentrations of 40 mmol/L or Fer-1, the ultrastructure of the cells was photographed by TEM.

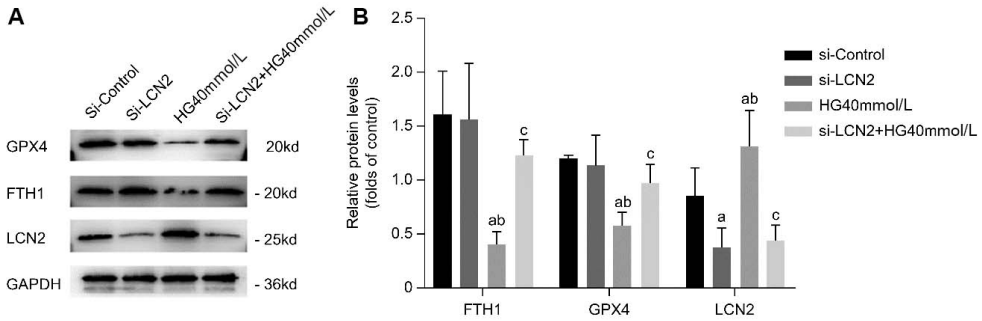

Fig. 4 Silencing of LCN2 alleviates ferroptosis in B-3 cells

(A-B) Results of Western blot analysis of GPX4, FTH1 and LCN2 of B-3 cells for four groups of si-Control, si-LCN2, 40 mmol/L high glucose, and si-LCN2 + 40 mmol/L high glucose. The results are presented from three independent experiments. (a: Compared with the si-Control group, b: Compared with the si-LCN2 group, c: Compared with the 40 mmol/L high glucose group, all $P < 0.05$).

ing SD rats for *in vivo* validation. The diabetic group exhibited significantly elevated blood glucose levels 72 h after STZ injection, with FBG exceeding 16. 7 mmol/L, confirming successful modeling. The diabetic rats maintaining high FBG and low body weight throughout the study. Compared with the control group, diabetic rats displayed typical diabetes symptoms, including increased water intake, food consumption, and urine output, weight loss, irritability, depression, and dry fur. From 1-12 weeks post-STZ injection, blood sugar levels gradually stabilized and decreased, while body weight continued to decline. Details of animal weight and blood sugar levels are presented in Table 2 and illustrated in Fig. 5A and B.

Lens opacification in the diabetic rats developed slowly from 4 to 8 weeks, with some lenses showing damage. The process accelerated from 8 to 12 weeks, leading to most lenses becoming completely opaque, while lenses in the control group remained transparent throughout the study (Fig. 5C).

3.6 Ferroptosis and LCN2 expression in the lens epithelial cells of DC rats

Based on the results, prolonged repeated ocular subconjunctival injections did not significantly impact the lens. Notably, rats treated with Fer-1 showed fewer cloudy lenses compared to the DC rats, with only mild cortical opacity observed at the equator (Fig. 6D). Anterior capsule samples from the three groups were analyzed for iron ions and protein expression levels of FTH1, GPX4, and LCN2 using IHC staining and Western blotting. The DC group exhibited significantly higher levels of these proteins compared to the DMSO group. However, Fer-1 treatment restored protein levels in DC rats (Fig. 6A, B), consistent with IHC staining results (Fig. 6E, F). Additionally, Fe^{2+}/Fe^{3+} levels in the anterior capsule of the lens confirmed the role of iron overload in DC progression (Fig. 6C). These findings suggest that ferroptosis may occur in the lens epithelial cells of DC rats, and that Fer-1 can significantly inhibit ferroptosis and delay cataract development s.

3.7 LCN2 silencing in the anterior segment of SD rats reduces ferroptosis and delays the development of DC

To further investigate whether differential expression of the LCN2 protein can delay the progression of DC by affecting ferroptosis, we constructed an *in vivo* DC rat model experiment. The study included 10 control rats and 10 rats with DC. Disease modeling followed standard protocols, with the modification that we used local tissue transfection reagents for eye injections to partially knockdown LCN2 in the rat anterior segment. The results showed trends consistent with previous modeling experiments in terms of diabetes symptoms, fasting glucose levels, and body mass (Fig. 7A, B) (Table 3). However, a detailed examination of the rat eyes revealed that, at the same time point, the DC group exhibited a significant reduction in lens opacity in the right eye compared to the left eye. In contrast, the control group maintained transparency in both eyes, and low LCN2 expression significantly reduced lens opacity (Fig. 7E). LCN2 and the ferroptosis-related cytokines GPX4 and FTH1 were analyzed at the protein level. The results indicated that the local knockdown efficiency of the LCN2 gene was high. In the control rats, there was no significant difference in the expression levels of FTH1 and GPX4 between the anterior lens capsules of the left and right eyes. However, in the DC rats, the expression of FTH1 and GPX4 was significantly higher in the anterior lens capsule of the right eye compared to the left eye (Fig. 7C, D). This pattern was also observed in immunohistochemical (IHC) staining of the anterior lens capsule, where the average OD of FTH1 and GPX4 did not differ significantly between the left and right eyes in the control group. In contrast, in the DC group, the average OD of FTH1 and GPX4 was significantly greater in the right eye compared to the left eye (Fig. 7F, G). These findings suggest that LCN2 knockdown reduces ferroptotic stress in lens epithelial cells of DC rats and delays the progression of DC.

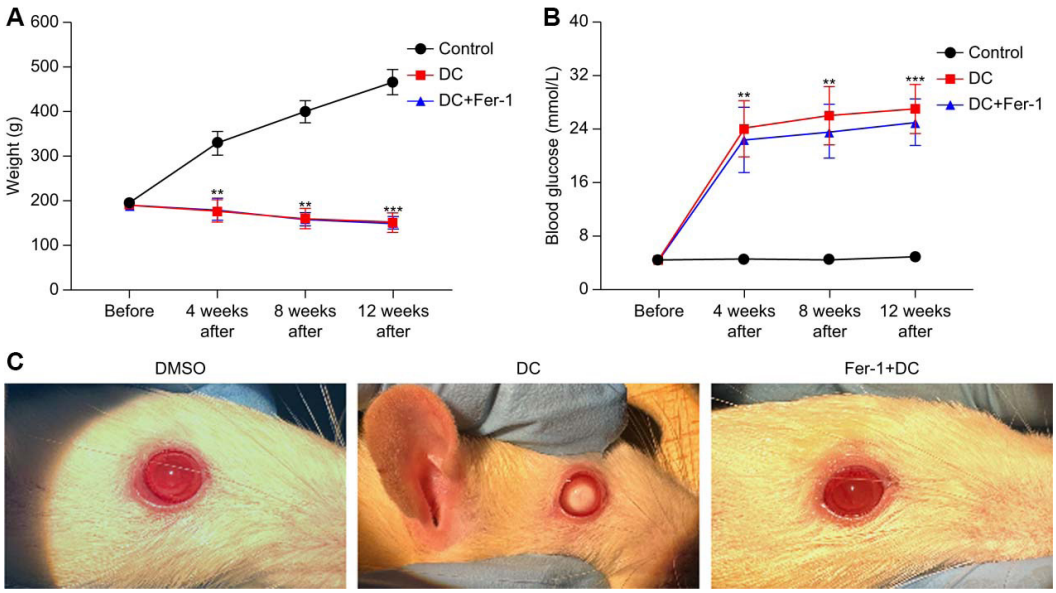

Fig. 5 Development of DC model in SD rats

(A-B) The results of fasting blood glucose (mmol/L) and body weight (g) were measured before modeling, 4 weeks after modeling, 8 weeks after modeling and 12 weeks after modeling in the three groups of SD rats, they were DMSO group, DC group and Fer-1 treatment group. ($^{**}P < 0.01$; $^{***}P < 0.005$). (C) The eye images of SD rats in the DMSO group, DC group and Fer-1 treatment group were taken after pupil dilation at 12 weeks after modeling.

Table 2 Comparison of weight and fasting blood glucose values of SD rats

Index	Control (*N* = 20)	DC (*N* = 20)	DC+Fer-1 (*N* = 20)	*F*	*P*
Weight (g)					
Before modeling	193.65 ± 7. 51	192. 35±6. 04	190. 7±4. 51	1. 16	0. 321
4 weeks after modeling	330. 73 ± 26. 64[b]	177. 48±25. 25[a, b]	180. 75±24. 66[a]	235. 18	< 0. 001
8 weeks after modeling	400. 82 ± 25. 26[b, c]	159. 94 ± 23. 25[a, b, c]	155. 71 ± 17. 39[a, b, c]	797. 68	< 0. 001
12 weeks after modeling	465. 42 ± 28. 54[b, c, d]	151. 47 ± 21. 5[a, b, c, d]	147. 05 ± 17. 77[a, b, c, d]	1255. 35	< 0. 001
Blood glucose (mmol/L)					
Before modeling	4. 50 ± 0. 36	4. 51 ± 0. 42	4. 48 ± 0. 35	0. 033	0. 968
4 weeks after modeling	4. 71 ± 0. 36[b]	24. 11 ± 4. 13[ab]	22. 46 ± 4. 81[a, b]	172. 15	< 0. 001
8 weeks after modeling	4. 53 ± 0. 72	26. 13 ± 4. 3[a, b, c]	24. 72 ± 4. 00[a, b, c]	249. 85	< 0. 001
12 weeks after modeling	5. 06 ± 0. 42[b, c, d]	27. 14 ± 3.63[a, b, c]	26. 13 ± 3. 42[a, b, c]	372. 13	< 0. 001

[a]Compared with the control group; [b]Compared with before modeling; [c]Compared with 4 weeks after modeling; [d]Compared to 8 weeks after modeling; SD, Sprague Dawley; DC, diabetic cataract

Table 3 Comparison of weight and fasting blood glucose values of SD rats

Index	Control (*N* = 10)	DC (*N* = 10)	*t*	*P*
Weight (g)				
Before modeling	196. 55 ± 7. 33	198. 51 ± 6. 26	0. 642	0. 529
4 weeks after modeling	331. 68 ± 42. 47[a]	178. 15 ± 11. 03[a]	11. 065	< 0. 001
8 weeks after modeling	405. 21 ± 29. 31[a, b]	156. 92 ± 16. 56[a]	23. 323	< 0. 001
12 weeks after modeling	470. 93 ± 32. 77[a, b, c]	143. 12 ± 14. 14[a, b, c]	29. 048	< 0. 001
Blood glucose (mmol/L)				
Before modeling	4. 64 ± 0. 37	4. 68 ± 0. 54	0. 194	0. 848
4 weeks after modeling	4. 55 ± 0. 41	23. 85 ± 5. 02[a]	12. 124	< 0. 001
8 weeks after modeling	4. 61 ± 0. 46	25. 08 ± 4. 53[a]	14. 224	< 0. 001
12 weeks after modeling	4. 74 ± 0. 34	26. 31 ± 3. 73[a]	18. 204	< 0. 001

[a]Compared with before modeling; [b]Compared with 4 weeks after modeling; [c]Compared with 8 weeks after modeling

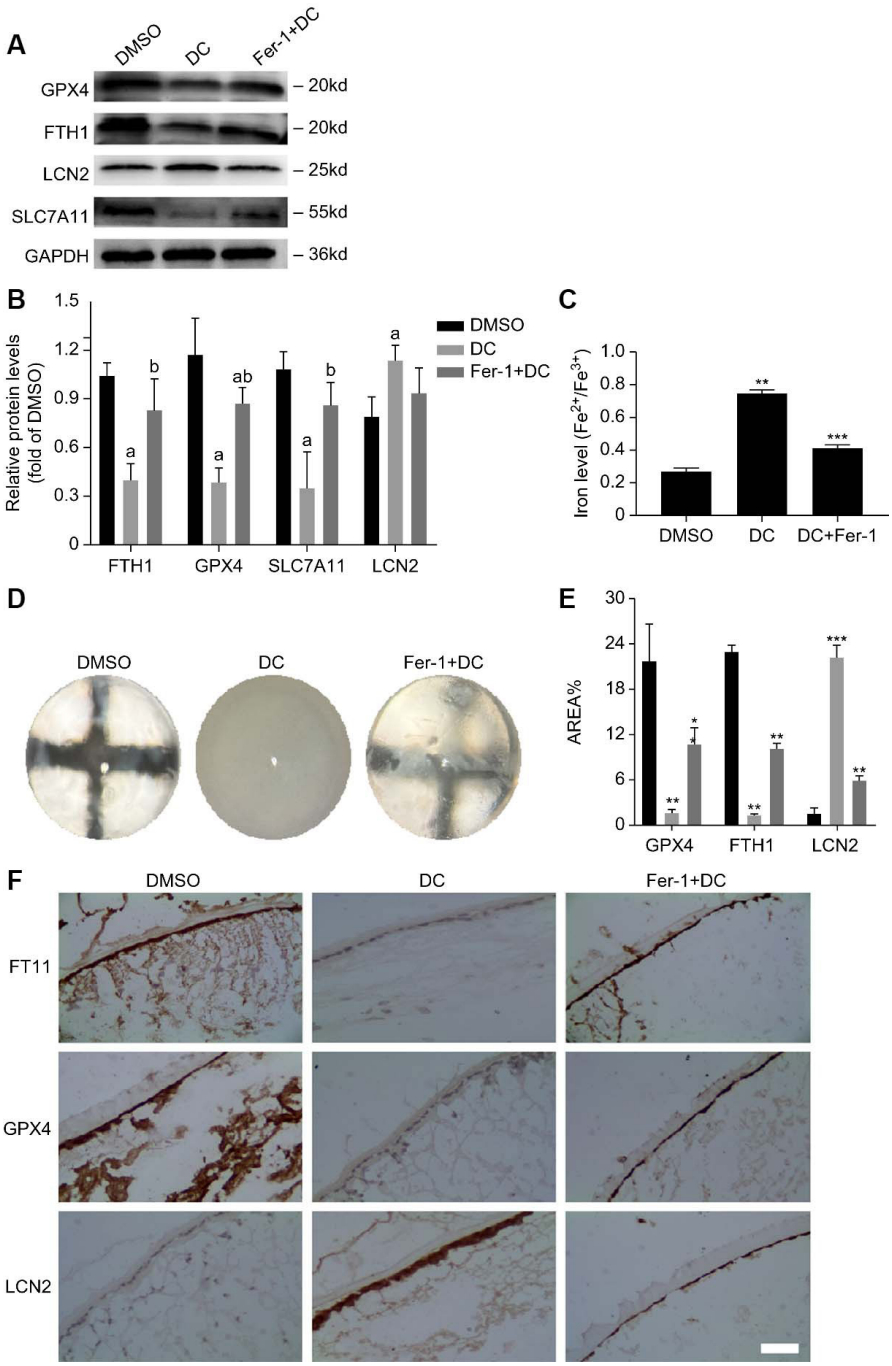

Fig. 6 Ferroptosis of lens epithelial cells isolated from SD rats with diabetes cataract

(A-B) They were three groups of SD rats (DMSO group, DC group and Fer-1 treatment group). The Western blot analysis results of GPX4, FTH1, LCN2, and SLC7A11 in the anterior capsule of their lenses. The results are presented from three independent experiments. (a: Compared with the DMSO group, b: : compared with the 40 mmol/L high glucose group, all $P < 0.05$). (C) They were three groups of SD rats (DMSO group, DC group and Fer-1 treatment group). The results of iron levels (Fe^{2+}/Fe^{3+}) in the anterior capsule of their lenses. The results are presented from three independent experiments. (D) They were three groups of SD rats (DMSO group, DC group and Fer-1 treatment group). These are pictures of their complete lenses taken out. (E-F) They were three groups of SD rats (DMSO group, DC group and Fer-1 treatment group). The average optical density of GPX4, FTH1, and LCN2 in their anterior capsule was measured using the IHC method (compared to DMSO). The results are presented from three independent experiments. ($^{*}P < 0.05$; $^{**}P < 0.01$; $^{***}P < 0.005$).

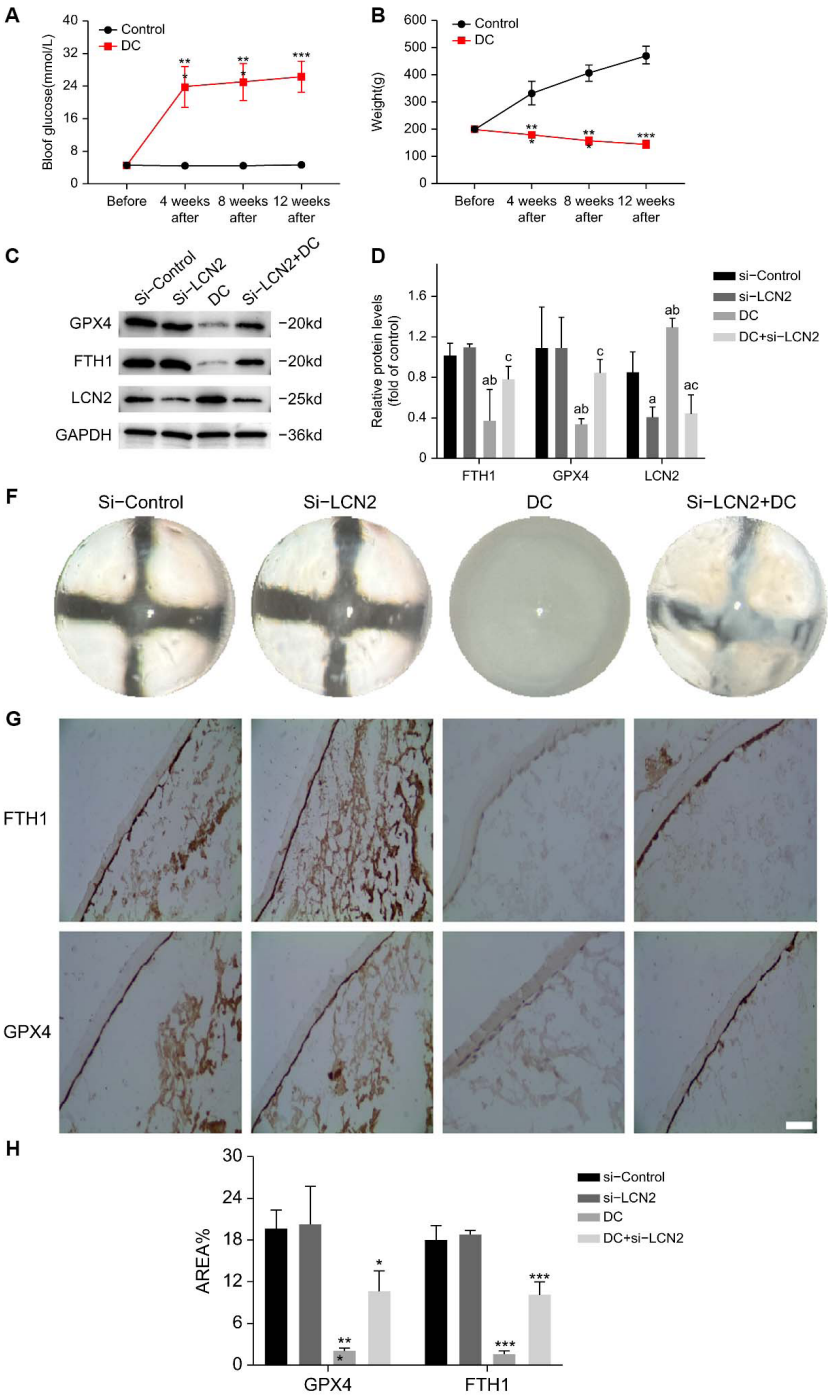

Fig. 7 LCN2 silencing inhibits ferroptosis in lens epithelial cells and delays the occurrence and development of diabetes cataract in anterior segment of SD rats

(A-B) The results of fasting blood glucose (mmol/L) and body weight (g) measured before modeling, 4 weeks after modeling, 8 weeks after modeling, and 12 weeks after modeling in SD rats of the Control and DC groups. (C-D) Western blot analysis of GPX4, FTH1, and LCN2 in the anterior capsule membrane of SD rats in four groups: si-Control, si-LCN2, DC, and si-LCN2+DC. The results are presented from three independent experiments. (a: Compared with the si-Control group, b: Compared with the si-LCN2 group, c: Compared with the DC group, all $P < 0.05$). (E) Complete lens images of four groups of SD rats: si Control, si-LCN2, DC, and si-LCN2+DC. (F-G) The average optical density of GPX4 and FTH1 was measured using IHC method for the anterior capsule of SD rats in four groups: si-Control, si-LCN2, DC, and si-LCN2+DC (compared to the si-Control group). The results are presented from three independent experiments. ($^{*}P < 0.05$; $^{**}P < 0.01$; $^{***}P < 0.005$).

4 Discussion

In this study, we conducted *in vitro* experiments using human lens epithelial cells treated with varying glucose concentrations. We found that glucose concentrations ranging from 5.5 to 40 mmol/L induced ferroptosis in these cells, with the severity of ferroptosis increasing with higher glucose levels. Importantly, ferroptosis was reversible with the treatment of Fer-1. In our *in vivo* experiments, we successfully established a stable rat model of DC. Compared to control SD rats, ferroptosis was observed in the lens epithelial cells of the DC group. However, pretreatment with Fer-1 mitigated the severity of ferroptosis in these cells, thereby slowing the progression of cataract development. Furthermore, we observed that LCN2 is normally expressed in human and rat lens epithelial cells. High glucose conditions significantly increased LCN2 expression in B-3 cells. Similarly, in DC rat models, LCN2 expression was notably elevated in lens epithelial cells. Targeting and silencing the LCN2 gene alleviated ferroptosis in both human and rat lens epithelial cells and slowed the onset and progression of DC. These findings suggest that LCN2 could serve as an early diagnostic marker for DC and may represent a promising new therapeutic target for the disease.

Establishing an accurate animal model to reflect the pathological processes of human diseases is essential for both basic and clinical research. For modeling DC, various methods can be employed[21-22]. To replicate the pathogenesis of DC effectively, a chemical inducer was used. The two most common chemical inducers for diabetes models are Alloxan (ALX) and STZ.

ALX induces hyperglycemia by inhibiting insulin receptors in the liver, reducing insulin secretion and increasing blood glucose levels[23]. While ALX is easy to use and inexpensive, it has the drawbacks of rapid onset and high efficacy, which can cause kidney damage and high mortality. STZ, an aminoglycoside compound, selectively destroys pancreatic islet β-cells, leading to insulin deficiency and hyperglycemia. It is applicable to various animal models, including mice, rats, and pigs. When used at controlled doses, STZ has lower mortality and is known for its long half-life, high model stability, and fast onset of disease. Additionally, STZ has lower tissue toxicity and mortality compared to ALX[24]. In this study, STZ was administered intraperitoneally to establish a DC animal model. Compared to the control group, the diabetic rat model exhibited significantly increased blood glucose levels, exceeding the standard (> 16.7 mmol/L) after injection. These rats also showed typical diabetes symptoms, including polydipsia, polyphagia, polyuria, reduced body mass, and a depressed state. Lens opacity developed gradually from 4 weeks, with a slow progression from 4-8 weeks and accelerated progression from 8-12 weeks. By the end of week 12, most rats displayed either cracks or complete opacity in their lenses. This experiment successfully established a stable DC animal model.

Recent advancements have significantly enhanced our understanding of ferroptosis mechanisms. Key players in ferroptosis inhibition include glutathione and GPX4, while phospholipid hydroperoxides act as executioners. Unrestricted lipid peroxidation is a hallmark of ferroptosis. This process begins with the extraction of hydrogen atoms from polyunsaturated fatty acid chains in the cell membrane's phospholipid bilayer, forming carbon-centered radicals. These radicals then react with molecular oxygen to produce peroxyl radicals[25]. If not effectively reduced to stable alcohols, these radicals perpetuate a chain reaction, generating numerous by-products that compromise the integrity of the cell membrane[26]. Phospholipid hydroperoxide production arises from various metabolic reactions. Jiang *et al.* explored how metabolism influences cell fate and uncovered a complex interplay between ferroptosis and cellular metabolism[27-29]. They discovered that cellular autophagy promotes ferroptosis by degrading iron-storage proteins, leading to increased destabilizing iron content within cells[30]. The role of mitochondria in ferroptosis further emphasizes the link between ferroptosis and cellular metabolism[31]. These studies highlight the intricate relationship between ferroptosis and metabolic pathways. Ferroptosis, a root cause of various diseases, offers several pharmacologically targetable points for therapeutic intervention. Over recent years, researchers have increasingly focused on ferroptosis and its connections to diverse diseases[32]. DM, a prevalent metabolic disorder, is associated with ferroptosis pathogenesis. Research indicates that ferroptosis plays a critical role in ischemia and reperfusion injury to the myocardium, kidneys, and retina in DM, contributing to diabetic cardiomyopathy, nephropathy, and retinopathy. The overproduction of ROS serves as a key link between ferroptosis and the development of these conditions[33]. Despite its prominence as a common ocular complication of diabetes, the relationship between ferroptosis and DC remains underexplored.

LCN2, a member of the lipid carrier protein family, was first identified in neutrophil granules in 1989[16]. It is expressed in immune cells and certain epithelial cells, acting as an acute-phase protein involved in rapid disease response and serving as an early diagnostic marker for various diseases[34-36]. Structurally, the bottom portion of LCN2 has hydrophobic amino acid residues that bind small lipophilic compounds, while its polar, positively charged residues can interact with macromolecules and hydrophilic compounds[37-38]. Under normal conditions, LCN2 is present in tissues such as the kidneys and lungs, where it plays a role in inhibiting bacterial infections by regulating iron levels[39-41]. Despite advances in understanding LCN2, its full range of functions remains unclear[42]. LCN2 is closely associated with acute inflammation and influences the host's inflammatory response. It can trigger inflammatory reactions on mucosal surfaces and is linked to various

pathological processes, including heart failure, alcoholic liver disease, and psoriasis, by recruiting neutrophils and inducing pro-inflammatory cytokine signaling[43-46]. Neutrophils and epithelial cells secrete large amounts of LCN2 in response to oxidative stress during inflammation, enhancing and maintaining the inflammatory response by attracting more neutrophils[47]. High LCN2 levels can further activate neutrophils and promote signaling pathways like MyD88 and NF-κB[48]. LCN2 interacts with multiple cell receptors to regulate iron metabolism, ferroptosis, pyroptosis, and inflammatory responses, impacting cell death and survival[49].

In this study, we discovered that LCN2 is expressed in both rat and human lens epithelial cells. High glucose levels significantly upregulated LCN2 expression in B-3 cells *in vitro*, but Fer-1 pretreatment reduced LCN2 levels to baseline. *In vivo*, LCN2 expression was significantly higher in the lens epithelial cells of SD rats with DC compared to controls, but Fer-1 treatment decreased LCN2 levels in the DC group. Mei *et al.* [42] also reported upregulated LCN2 in retinal ischemia-reperfusion models, which exacerbated retinal ferroptosis. These findings suggest that LCN2 may be an early biomarker for DC and play a crucial role in its pathogenesis, potentially influencing the severity of ferroptosis and the disease course.

Inflammation is a fundamental physiological response aimed at maintaining tissue homeostasis by counteracting various stimuli. However, when inflammation is dysregulated, it can lead to cell death. Investigating the interplay between ferroptosis and inflammation is crucial for uncovering broader pathophysiological mechanisms and identifying potential therapeutic targets for related diseases. Increasing evidence links iron metabolism with the activation of inflammation-related signaling pathways[50]. Dysregulation of the redox system can activate multiple pathways, with the pro-inflammatory cytokines produced exacerbating intracellular oxidative stress and lipid peroxidation, creating a vicious cycle. For instance, during ferroptosis in smooth muscle cells, NF-κB signaling is activated, leading to increased release of pro-inflammatory cytokines such as chemokines and colony-stimulating factors[51]. Antioxidant inhibition of ferroptosis in a choline-deficient, ethionine-supplemented dietary model reduced pro-inflammatory cytokine release and alleviated liver injury[52]. Several inflammation-related signaling pathways, including the inflammasome, NF-κB, JAK-STAT, cGAS-STING, and MAPK pathways, can induce ferroptosis.

The inflammasome is a protein complex, with NLRP3 being the most extensively studied[53]. NLRP3 detects specific stimuli and initiates the formation of downstream signaling complexes, triggering the activation of caspase-1. Activated caspase-1 processes pro-inflammatory cytokines, interleukin-1β and interleukin-18, into their active forms and secretes them to amplify the inflammatory response. Additionally, caspase-1 cleaves the pore-forming protein GSDMD, creating pores in the cell membrane, leading to cytokine release and pyroptotic cell death[54]. NLRP3 has been implicated in ferroptosis, with studies showing that LCN2 expression increases significantly during inflammation. LCN2 can bind to ATG4B, inhibiting autophagosome maturation[55]. This leads to iron accumulation within cells, driving NLRP3 activation through the cGAS-STING1 pathway, which in turn induces oxidative stress, lipid peroxidation, and ferroptosis[54]. Ferroptosis inducers like erastin can activate NLRP3, exacerbating these processes, while inhibitors like Fer-1 can suppress NLRP3 activation, reversing the effects and delaying disease progression[56]. Additionally, NLRP1 activation has been observed during ferroptosis[57].

These findings suggest that inflammasome formation, particularly involving NLRP3, is a critical step in ferroptosis, with LCN2 playing a significant role in this process. To further explore how LCN2 expression influences ferroptosis, we investigated changes in ferroptosis-related factors GPX4 and FTH1 through targeted silencing of the LCN2 gene in both *in vivo* and *in vitro* experiments. We also assessed lens opacity in rats. Our results indicated that silencing the LCN2 gene delayed DC development and partially alleviated ferroptosis. This is consistent with findings by Luo *et al.* [58], suggesting that low levels of LCN2 in the disease model might mitigate the inflammatory response, reduce ferroptosis, and ultimately delay cataract formation.

Diabetes prevalence is notably higher in northern regions compared to the south, potentially due to long-term cold environments affecting serum levels of iron, glucose, HbA1c, TG, LDL, and HDL, which are closely linked to oxidative stress. Studies indicate that fasting blood glucose levels in diabetes patients are higher in winter than in spring and autumn, with summer showing the lowest levels. Cold exposure stimulates sympathetic nerve activity, increases catecholamine secretion, raises blood glucose levels, and can worsen the disease and induce complications. Diabetes, a chronic condition, leads to numerous complications over time, with DC being the most common ocular complication. Our *in vitro* and *in vivo* experiments reveal that ferroptosis plays a crucial role in the pathogenesis of DC, and LCN2 could be a promising new therapeutic target for this condition.

5 Conclusion

Our findings indicate that LCN2 is expressed in lens epithelial cells and is significantly upregulated during the progression of DC. Targeted silencing of the LCN2 gene effectively inhibited iron-dependent cell death, thereby delaying the development of DC. These results highlight LCN2's potential as both a diagnostic biomarker and a novel therapeutic target for DC. Future research will focus on screening effective compounds to selectively inhibit

LCN2 activation, with the aim of achieving therapeutic or even preventive effects against DC.

Author contributions

Ge H Y and Zhang J Y designed the study. Zhang J Y, Yu X H and Yang C conducted *in vitro* experiments. Zhang J Y, Sun L Y and Wei C Q conducted *in vivo* experiments. Ge H Y guided and supervised this study. Zhang J Y wrote the manuscript. Ge H Y and Sun L Y revised the manuscript. All authors have contributed to the submitted version of the manuscript.

Source of funding

This research was funded by the Horizontal Scientific Research Project of Harbin Medical University (grant number: 2022HX005). The funders played an important role in the research design and study publication decisions.

Ethical Approval

The study was approved by the Institutional Review Board (or Ethics Committee) of the First Affiliated Hospital of Harbin Medical University (IACUC: 2022020 and date of approval: April 8, 2022).

Informed consent

Not Applicable.

Conflict of interest

The authors declare no conflicts of interest.

Data availability statement

Data used to support the findings of this study are available from the corresponding author upon request.

References

[1] World Health Organization. Health Topics/Diabetes. https: //www. who. int/health-topics/. Accessed on May 27, 2021.
[2] Liu Y C, Wilkins M, Kim T, *et al.* Cataracts. Lancet, 2017; 390(10094): 600-612.
[3] Thiagarajan R, Manikandan R. Antioxidants and cataract. Free Radic Res, 2013; 47(5): 337-345.
[4] Murtha T, Cavallerano J. The management of diabetic eye disease in the setting of cataract surgery. Curr Opin Ophthalmol, 2007; 18(1): 13-18.
[5] Foster P J, Wong T Y, Machin D, *et al.* Risk factors for nuclear, cortical and posterior subcapsular cataracts in the Chinese population of Singapore: The tanjong pagar survey. Br J Ophthalmol, 2003; (9): 1112-1120.
[6] Nirmalan P K, Robin A L, Katz J, *et al.* Risk factors for age related cataract in a rural population of southern India: The aravind comprehensive eye study. Br J Ophthalmol. 2004; 88(8): 989-994.
[7] Husain R, Tong L, Fong A, *et al.* Prevalence of cataract in rural Indonesia. Ophthalmology, 2005; 112(7): 1255-1262.
[8] Dandona L, Dandona R, Naduvilath T J, *et al.* Population-based assessment of the outcome of cataract surgery in an urban population in southern India. Am J Ophthalmol, 1999; 127(6): 650-658.
[9] Chen S J, Liu J H, Shih H C, *et al.* Prevalence and associated factors of lens opacities among Chinese type 2 diabetics in Kinmen, Taiwan. Acta Diabetol, 2008; 45(1): 7-13.
[10] Starr M R, Mahr M A, Smith W M, *et al.* Outcomes of patients with active diabetic macular edema at the time of cataract surgery managed with intravitreal anti-vascular endothelial growth factor injections. Am J Ophthalmol, 2021; 229(9): 194-199.
[11] Chen X, Yu C, Kang R, *et al.* Iron metabolism in ferroptosis. Front Cell Dev Biol, 2020; 8(10): 590226.
[12] Dixon S J, Lemberg K M, Lamprecht M R, *et al.* Ferroptosis: an iron-dependent form of nonapoptotic cell death. Cell, 2012; 149(5): 1060-1072.
[13] Zhao Y, Pan B, Lv X, *et al.* Ferroptosis: roles and molecular mechanisms in diabetic cardiomyopathy. Front Endocrinol, 2023; 14(4): 1140644.
[14] Huang Q, Tian H, Tian L, *et al.* Inhibiting Rev-erbα-mediated ferroptosis alleviates susceptibility to myocardial ischemia-reperfusion injury in type 2 diabetes. Free Radic Biol Med, 2023; 209(11): 135-150
[15] Wu Y, Chen Y. Research progress on ferroptosis in diabetic kidney disease. Front. Endocrinol, 2022; 29(9): 945976
[16] Abella V, Scotece M, Conde J, *et al.* The potential of lipocalin-2/NGAL as biomarker for inflammatory and metabolic diseases, Biomarkers. 2015; 20(8): 565-71.
[17] El Shahawy M S, Hemida M H, Abdel-Hafez H A, *et al.* Urinary neutrophil gelatinase-associated lipocalin as a marker for disease activity in lupus nephritis, Scand. J Clin Lab Invest, 2018; 78(4): 264-268.
[18] Wells J M, Brummer R J, Derrien M, *et al.* Homeostasis of the gut barrier and potential biomarkers. Am J Physiol Gastrointest Liver Physiol, 2017; 312(3): G171-G193.
[19] Shao S, Fang H, Dang E, *et al.* Neutrophil extracellular traps promote inflammatory responses in psoriasis *via* activating epidermal TLR4/IL-36R crosstalk. Front Immunol, 2019; 10(4): 746.
[20] Javaid H M A, Ko E, Joo E J, *et al.* TNFα-induced NLRP3 inflammasome mediates adipocyte dysfunction and activates macrophages through adipocyte-derived lipocalin 2. Metabolism, 2023; 142(5): 155527.
[21] Asdaq S M B, Mannasaheb B A, Orfali R, *et al.* Antidiabetic and antioxidant potential of crocin in high-fat diet plus streptozotocin-induced type-2 diabetic rats. Int J Immunopathol Pharmacol, 2024; 38(11-12): 3946320231220178.

[22] Qiao Y Y, Ji J L, Hou W L, *et al.* tRF3-IleAAT reduced extracellular matrix synthesis in diabetic kidney disease mice by targeting ZNF281 and inhibiting ferroptosis. Acta Pharmacol Sin, 2024; 45(5): 1032-1043.
[23] El Maksoud A I A, Al-Karmalawy A A, ElEbeedy D, *et al.* Symbiotic antidiabetic effect of Lactobacillus casei and the bioactive extract of Cleome droserifolia (Forssk.) Del. on mice with type 2 diabetes induced by alloxan. Chem. Biodivers, 2024; 21(1): e202301397.
[24] Goyal S N, Reddy N M, Patil K R, *et al.* Challenges and issues with streptozotocin-induced diabetes - A clinically relevant animal model to understand the diabetes pathogenesis and evaluate therapeutics. Chem Biol Interact, 2016; 224(1): 49-63.
[25] Conrad M, Pratt D A. The chemical basis of ferroptosis. Nat. Chem Biol, 2019; 15(12): 1137-1147.
[26] Jiang X, Stockwell B R, Conrad M. Ferroptosis: Mechanisms, biology and role in disease, Nat. Rev. Mol Cell Biol. 2021; 22(4): 266-282.
[27] Gao M, Monian P, Quadri N, *et al.* Glutaminolysis and transferrin regulate ferroptosis. Mol Cell, 2015; 59(2): 298-308.
[28] Gao M, Monian P, Pan Q, *et al.* Ferroptosis is an autophagic cell death process. Cell Res, 2016; 26(9): 1021-1032.
[29] Gao M, Yi J, Zhu J, *et al.* Role of mitochondria in ferroptosis. Mol Cel, 2019; 73(2): 354-363. e3.
[30] Hou W, Xie Y, Song X, *et al.* Autophagy promotes ferroptosis by degradation of ferritin. Autophagy, 2016; 12(8): 1425-1428.
[31] Tan S, Schubert D, Maher P. Oxytosis: a novel form of programmed cell death, Curr. Top Med Chem, 2001; 1(6): 497-506.
[32] Chen Y, Fang Z M, Yi X, *et al.* The interaction between ferroptosis and inflammatory signaling pathways. Cell Death Dis, 2023; 14(3): 205.
[33] Li S, Lu S, Wang L, *et al.* Effects of amygdalin on ferroptosis and oxidative stress in diabetic retinopathy progression *via* the NRF2/ARE signaling pathway. Exp Eye Res, 2023; 234(9): 109569.
[34] Devireddy L R, Gazin C, Zhu X, *et al.* A cell-surface receptor for lipocalin 24p3 selectively mediates apoptosis and iron uptake. Cell, 2005; 123(7): 1293-1305.
[35] Ellermann M, Arthur J C. Siderophore-mediated iron acquisition and modulation of host-bacterial interactions. Free Radic Biol Med, 2017; 105(4): 68-78.
[36] Li D, Yan Sun W, Fu B, *et al.* Lipocalin-2-The myth of its expression and function. Basic Clin Pharmacol Toxicol. 2020; 127(2): 142-151.
[37] Goetz D H, Willie S T, Armen R S, *et al.* Ligand preference inferred from the structure of neutrophil gelatinase associated lipocalin. Biochemistry, 2000; 39(8): 1935-1941.
[38] Xiao X, Yeoh B S, Vijay-Kumar M. Lipocalin 2: An emerging player in iron homeostasis and inflammation. Annu. Rev Nutr, 2017; 37(8): 103-130.
[39] Dahl S L, Woodworth J S, Lerche C J, *et al.* Lipocalin-2 functions as inhibitor of innate resistance to Mycobacterium tuberculosis. Front Immunol, 2018; 9(11): 2717.
[40] Guglani L, Gopal R, Rangel-Moreno J, *et al.* Lipocalin 2 regulates inflammation during pulmonary mycobacterial infections. PLoS One, 2012; 7(11): e50052.
[41] Saiga H, Nishimura J, Kuwata H, *et al.* Lipocalin 2-dependent inhibition of mycobacterial growth in alveolar epithelium. J Immunol, 2008; 181(12): 8521-8527.
[42] Mei T, Wu J, Wu K, *et al.* Lipocalin 2 induces visual impairment by promoting ferroptosis in retinal ischemia-reperfusion injury. Ann Transl Med, 2023; 11(1): 3.
[43] Wu H, Santoni-Rugiu E, Ralfkiaer E, *et al.* Lipocalin 2 is protective against E. coli pneumonia, Respir Res, 2010; 11(1): 96.
[44] Warszawska J M, Gawish R, Sharif O, *et al.* Lipocalin 2 deactivates macrophages and worsens pneumococcal pneumonia outcomes. J Clin Invest, 2013; 123(8): 3363-3372.
[45] Rahimi S, Roushandeh A M, Ahmadzadeh E, *et al.* Implication and role of neutrophil gelatinase-associated lipocalin in cancer: Lipocalin-2 as a potential novel emerging comprehensive therapeutic target for a variety of cancer types. Mol. Biol Rep, 2020; 47(1): 2327-2346.
[46] Wang Y, Jia M, Yan X, *et al.* Increased neutrophil gelatinase-associated lipocalin (NGAL) promotes airway remodelling in chronic obstructive pulmonary disease. Clin Sci (Lond), 2017; 131(11): 1147-1159.
[47] Ghosh S, Stepicheva N, Yazdankhah M, *et al.* The role of lipocalin-2 in age-related macular degeneration (AMD). Cell. Mol Life Sci, 2020; 77(5): 835-851.
[48] Guardado S, Ojeda-Juárez D, Kaul M, *et al.* Comprehensive review of lipocalin 2-mediated effects in lung inflammation. Am J Physiol Lung Cell Mol Physiol, 2021; 321(4): L726-L733.
[49] Tang W, Ma J, Gu R, *et al.* Light-induced lipocalin 2 facilitates cellular apoptosis by positively regulating reactive oxygen species/Bim signaling in retinal degeneration. Invest Ophthalmol Vis Sci, 2018; 59(12): 6014-6025.
[50] Chen X, Kang R, Kroemer G, *et al.* Ferroptosis in infection, inflammation, and immunity. J Exp Med, 2021; 218(6): e20210518.
[51] Chen Y, Yi X, Huo B, *et al.* BRD4770 functions as a novel ferroptosis inhibitor to protect against aortic dissection, Pharmacol Res, 2022; 177(5): 106122.
[52] Tsurusaki S, Tsuchiya Y, Koumura T, *et al.* Hepatic ferroptosis plays an important role as the trigger for initiating inflammation in nonalcoholic steatohepatitis. Cell Death Dis, 2019; 10(6): 449.
[53] Schnappauf O, Chae J J, Kastner D L, *et al.* The pyrin inflammasome in health and disease. Front. Immunol, 2019; 10(8): 1745.
[54] Chauhan D, Vande Walle L, Lamkanfi M. Therapeutic modulation of inflammasome pathways. Immunol Rev, 2020; 297(1): 123-138.
[55] Gupta U, Ghosh S, Wallace C T, *et al.* Increased LCN2 (lipocalin 2) in the RPE decreases autophagy and activates inflammasome-ferroptosis processes in a mouse model of dry AMD. Autophagy, 2023; 19(1): 92-111.
[56] Xie S S, Deng Y, Guo S L, *et al.* Endothelial cell ferroptosis mediates monocrotaline-induced pulmonary hypertension in rats by modulating NLRP3 inflammasome activation. Sci. Rep, 2022; 12(1): 3056.
[57] Meihe L, Shan G, Minchao K, *et al.* The Ferroptosis-NLRP1 inflammasome: The vicious cycle of an adverse pregnancy. Front Cell Dev Biol, 2021; 9(8): 707959.
[58] Luo L, Deng L, Chen Y, *et al.* Identification of lipocalin 2 as a ferroptosis-related key gene associated with hypoxic-ischemic brain damage *via* STAT3/NF-κB signaling pathway. Antioxidants (Basel), 2023; 12(1): 186.